The Journal of Neuroscience, April 15, 1996, 16(8):2532–2545

Whole-Cell Chloride Currents in Rat Astrocytes Accompany Changes in Cell Morphology

Christopher D. Lascola[1] and Richard P. Kraig[1,2]

[1]Committee on Neurobiology and [2]Departments of Neurology and Pharmacological and Physiological Sciences, The University of Chicago, Chicago, Illinois 60637

Astrocytes can change shape dramatically in response to increased physiological and pathological demands, yet the functional consequences of morphological change are unknown. We report the expression of Cl^- currents after manipulations that alter astrocyte morphology. Whole-cell Cl^- currents were elicited after (1) rounding up cells by brief exposure to trypsin; (2) converting cells from a flat polygonal to a process-bearing (stellate) morphology by exposure to serum-free Ringer's solution; and (3) swelling cells by exposure to hypo-osmotic solution. Zero-current potentials approximated the Nernst for Cl^-, and rectification usually followed that predicted by the constant-field equation. We observed heterogeneity in the activation and inactivation kinetics, as well as in the relative degree of outward versus inward rectification. Cl^- conductances were inhibited by 4,4-diisothiocyanostilbene-2,2′-disulfonic acid (200 μM) and by Zn^{2+} (1 mM). Whole-cell Cl^- currents were not expressed in cells without structural change.

We investigated whether changes in cytoskeletal actin accompanying changes in astrocytic morphology play a role in the induction of shape-dependent Cl^- currents. Cytochalasins, which disrupt actin polymers by enhancing actin-ATP hydrolysis, elicited whole-cell Cl^- conductances in flat, polygonal astrocytes. In stellate cells, elevated intracellular Ca^{2+} (2 μM), which can depolymerize actin, enhanced Cl^- currents, and high intracellular ATP (5 mM), required for repolymerization, reduced Cl^- currents. Modulation of Cl^- current by Ca^{2+} and ATP was blocked by concurrent whole-cell dialysis with phalloidin and DNase, respectively. Phalloidin stabilizes actin polymers and DNase inhibits actin polymerization. Dialysis with phalloidin also prevented hypo-osmotically activated Cl^- currents. These results demonstrate how the expression of astrocyte Cl^- currents can be dependent on cell morphology, the structure of actin, Ca^{2+} homeostasis, and metabolism.

Key words: astrocyte; chloride current; morphology; actin; calcium; ATP

Changes in astrocyte morphology are a hallmark of virtually all pathological events in brain (Ransom and Kettenmann, 1995). These morphological changes can include hypertrophy (Petito et al., 1990), process elaboration and reorientation (Mathewson and Berry, 1985), and/or swelling (Kimelberg et al., 1989). Changes in astrocyte shape are also seen with less injurious perturbations (Kraig et al., 1991) and even accompany physiological processes such as motor learning (Anderson et al., 1994.) The relationship between cell shape and astrocyte function, however, remains poorly understood.

One astrocyte function that may change with alterations in cell shape is ion homeostasis. Changes in the expression of several astrocyte ion conductances follow exposure to dibutyryl cAMP (Barres et al., 1989) and phorbol esters (Backus et al., 1991), and also occur during coculture with neurons (Corvalan et al., 1990), all conditions that transform cultured astrocytes from a flat, polygonal to a process-bearing (stellate) morphology (Levison and McCarthy, 1991). In addition, osmotic swelling in cultured astrocytes seems to induce a Cl^- permeability requisite for regulatory volume decrease (RVD) (Pasantes-Morales et al., 1994).

Astrocytic ion homeostasis inevitably involves the movement of Cl^-. Cl^- serves as an important counter anion to K^+ uptake and is a transported species on ion exchangers and cotransporters carrying H^+ equivalents (Kimelberg et al., 1986). Although increases in intracellular Cl^- concentration ($[Cl^-]_i$) accompanying astroglial depolarization (Ballanyi et al., 1987; Walz and Mukerji, 1988) suggest the presence of electrogenic Cl^- transport, reports of single anion channels in resting astrocytes indicate that Cl^- channels are normally not functional. Channel activity requires excision of the membrane patch (Barres et al., 1990b) and, in the case of large-conductance anion channels, on the proximity of the membrane potential to 0 mV (Sonnhof, 1987) and/or the zero-current potential (Jalonen, 1993). In one series of reports, however, Bevan et al. (1985) and Gray and Ritchie (1986) observed voltage-dependent whole-cell Cl^- currents activated at potentials more positive than −50 mV.

We used the whole-cell patch-clamp technique to reexamine Cl^- currents in rat type-1 neocortical cultured astrocytes and to determine whether whole-cell current expression depends on changes in cell morphology. Consistent with most studies (for review, see Barres et al., 1990b), we did not observe any Cl^- conductance in control astrocytes with a flat, polygonal morphology. In contrast, cells expressed whole-cell Cl^- currents after being rounded up by brief exposure to trypsin, a technique used by

Received Nov. 21, 1995; revised Jan. 5, 1996; accepted Jan. 10, 1996.

This work was supported by grants from the National Institute of Neurological Disorders and Stroke (NS-19108), the American Heart Association of Metropolitan Chicago, and the Brain Research Foundation of The University of Chicago. C.D.L. was supported by an MD/PhD Training Grant in Growth and Development (HD-07009) from the National Institute of Child Health and Human Development, and a National Research Service Award (F31-MH11126) from the National Institute of Mental Health. We thank Dr. Deborah Nelson, Dr. Philip Kunkler, and Anthony Caggiano for helpful discussions and for reading this manuscript, Marcia Kraig for assistance with tissue culture preparation, and Raymond Hulse for image enhancement and restoration.

Correspondence should be addressed to Richard P. Kraig, Department of Neurology, MC 2030, University of Chicago, 5841 South Maryland Avenue, Chicago, IL 60637.

Gray and Ritchie (1986) in their experiments to facilitate patch-clamp recording. Additional experiments demonstrated that other alterations in astrocytic shape, i.e., transformation from flat to stellate by exposure to serum-free Ringer's solution and osmotic swelling, also elicited Cl^- currents.

Changes in astrocytic morphology can involve changes in the actin cytoskeleton (Goldman and Abramson, 1990; Baorto et al., 1992). Moreover, cytoskeletal actin is functionally and structurally associated with several ion channels (Guharay and Sachs, 1984; Srinivasan et al., 1988; Hudspeth, 1989; Cantiello et al., 1991; Fröehner, 1991; Johnson and Byerly, 1993; Rosenmund and Westbrook, 1993; Suzuki et al., 1993; Haussler et al., 1994; Schwiebert et al., 1994; Levitan et al., 1995). Accordingly, we investigated whether changes in actin play a role in shape-dependent Cl^- current expression. Modulation of Cl^- conductances by cytochalasins, Ca^{2+}, ATP, phalloidin, and DNase, all agents that act on the actin cytoskeleton, demonstrated how changes in the state of actin polymerization may underlie the expression of shape-dependent Cl^- current expression in cultured astrocytes and how Cl^- currents may ultimately be controlled by $[Ca^{2+}]_i$ and energy supply, two physiological parameters inextricably linked to astrocyte functions within the nervous system.

MATERIALS AND METHODS

Cell culture preparation. Neocortical type-1 astrocytes were prepared and purified from primary cultures of neonatal rat brain by a modification of the methods of McCarthy and de Vellis (1980). Brains were removed from halothane-anesthetized 0- to 2-d-old rat pups and stripped of their meninges. Portions of both frontal and parietal cortices were dissected, and any remaining meninges and blood vessels were carefully removed. The cortical tissue was minced to 1 mm pieces with a scalpel blade in cold (4–10°C) HBSS and was mechanically dissociated further by sequential passage through 18, 20, 24, and 26 gauge needles, with final passage through a 53 mM Nytex screen. The cells were centrifuged at $150 \times g$ for 7 min; the pellet was resuspended in DMEM with 10% fetal calf serum, and the cells were plated in 25 cm^2 flasks. The medium was changed initially at 24 hr and then once every 4–5 d thereafter. At 7–10 d, the culture consisted of a top layer of type-2-like astrocytes, glial progenitor cells, and microglia residing on a confluent layer of neocortical type-1 astrocytes (Levison and McCarthy, 1991). After 3–6 weeks, the cells on the confluent layer were removed using a variant of the "shaking off" procedure (McCarthy and de Vellis, 1980). Culture flasks were shaken vigorously at 225 rpm for 20 hr; their media were refreshed and then reshaken for another 20 hr. The type-1-like cells were trypsinized (0.025%) from the flask and replated at lower densities onto alcohol- and flame-sterilized 25 mm diameter round coverslips. The final cultures consisted of 98% pure neocortical type-1 astrocytes, based on immunohistochemical labeling with markers to glial fibrillary acidic protein (GFAP) and A2B5 (type-2-like astrocytes), as well as DiI-Ac-LDL inclusion by microglia. Electrophysiological recordings were made between days 3 and 12 after replating and before cells became confluent.

Immunohistochemical and cytochemical characterization. Staining of cytoskeletal actin and GFAP was carried out as follows. Astrocytes were rinsed three times in PBS and then fixed with acetone for 15 min at −20°C. After three washes in PBS, cells were incubated for 30 min in PBS containing 3% normal goat serum and 0.25% Triton X-100 (PBS-X). Cells were then incubated for 1 hr in PBS-X containing either primary antibody to GFAP at 1:50 dilution or fluorescein isothiocyanate (FITC)-conjugated phalloidin (for actin) at 1:10 dilution of a 26.4 mM stock solution (methanol as solvent.) After several rinses with PBS-X, cells stained for GFAP were incubated for 30 min with a rhodamine-conjugated secondary antibody. After three final washes in PBS, coverslips were mounted onto slides using aqueous gel-mount and examined for immunofluorescence.

For A2B5, cells were washed three times in PBS and then fixed with 4% paraformaldehyde for 15 min. PBS containing 3% normal goat serum and no Triton X-100 (PBS-GS) was used for 30 min of blocking incubation and as the diluent for the primary and secondary antibodies. A2B5 was used at 10 mg/ml. After several washes with PBS-GS, plates were incubated with an appropriate rhodamine-conjugated secondary antibody, washed again in PBS-GS, and mounted on slides with aqueous gel-mount.

For DiI-Ac-LDL microglial staining (Giulian and Baker, 1986), cells were washed several times in standard 150 mM NaCl Ringer's solution (for Ringer's recipe, see Solutions) and then incubated in Ringer's solution containing DiI-Ac-LDL at a concentration of 10 mg/ml. Plates were examined for immunofluorescence without fixation.

Illustrations were prepared from electronic images in accord with recent discussions (Anderson, 1994). Fluorescent images were photographed using 100 ASA Ektachrome film (Eastman Kodak, Rochester, NY) with an Orthomat E automatic exposure unit (Leica, St. Gallen, Switzerland) and a Laborlux D compound microscope (Leica). Resultant slides were transformed into electronic files using a Kodak Professional Film Scanner (model 2035, Eastman Kodak) at 1000 pixels/inch. Electronic images were processed using Image Pro Plus software (version 1.3; Media Cybernetics, Silver Spring, MD). First, images were refocused using a "hi Gaussian" filter [7×7 pixel matrix at 50% strength and two passes (see Fig. 1) and 100% strength and one pass (see Fig. 10)]. Second, image brightness was raised and background noise was lowered by applying brightness, contrast, and γ function values of 70, 60, and 0.5 to all pictures. Final images were printed using a dye sublimation printer (XLT-7720; Eastman Kodak).

Solutions. In most experiments, whole-cell currents were obtained using asymmetrical Cl^- solutions ($Nernst_{Cl^-} = -31$ mV), allowing us to identify an increase in leak conductance as a depolarizing shift in the zero-current potential. The pipette solution contained (in mM): 40 *N*-methyl-D-glucamine (NMDG)-Cl, 100 NMDG-gluconate, 2 $MgCl_2$, and 10 HEPES, and a Ca^{2+}-EGTA buffer to yield a desired free Ca^{2+} concentration buffered to pH 7.2. Ca^{2+}-EGTA buffer solutions were prepared according to the procedure described by Neher (1988), and final free Ca^{2+} concentrations were calculated assuming an apparent dissociation constant of the Ca^{2+}-EGTA complex of 0.15 mM at pH 7.2. Ca^{2+} concentrations for individual experiments are indicated in the text and figure legends. The bath solution contained (in mM): 140 NMDG-Cl, 2 $CaCl_2$, 2 $MgCl_2$, and 10 HEPES buffered to pH 7.4. Gluconate replaced Cl^- in Cl^- substitution experiments. The addition of ATP (as Mg^{2+} salt) and cytoskeletal reagents to either bath or pipette solutions is as indicated in the text and figure legends. Most incubations with or without pharmacological agents used a Ringer's solution as follows (in mM): 140 NaCl, 3 KCl, 1.5 $CaCl_2$, 1 $MgCl_2$, 10 dextrose, 10 HEPES, pH 7.4. Trypsin incubations were performed in divalent cation-free HBSS. Approximately half of our electrophysiological experiments were also carried out in the presence of 0.1 mM $LaCl_3$, which reduced low-frequency background current noise, perhaps stabilizing the seal between the pipette and the cell membrane (Nakao and Gadsby, 1989). Each experimental manipulation was carried out in both the presence and absence of $LaCl_3$. La^{3+}, a general cation conductance blocker, did not reduce or enhance Cl^- currents measured under any circumstances in our experiments. Pipette solution osmolarity was ~280 mOsm, and bath solutions were ~290 mOsm, unless indicated otherwise. Solution osmolarity was monitored using a vapor pressure osmometer (model 5500, Wescor, Logan, UT.)

Electrophysiology. Voltage-clamp experiments were carried out using the tight-seal, whole-cell variant of the patch-clamp technique as described by Hamill et al. (1981). Patch pipettes were fabricated from thin-walled borosilicate glass (outer diameter 1.5 mm, inner diameter 0.86 mm; A-M Systems, Everett, WA) and fire-polished immediately before recording to an inner tip diameter of 1–2 mM. In most experiments, pipettes were filled with a solution in which permeant monovalent cations were replaced by the relatively large, impermeant cation *N*-methyl-D-glucamine (NMDG), and a substantial fraction of permeant Cl^- was replaced with the relatively impermeable anion gluconate (see Solutions). Electrodes filled with this solution had resistances of 1.2 ± 0.04 MΩ ($n = 117$).

Glass coverslips containing cells at nonconfluent density were placed in a Leiden coverslip dish mounted into a movable open perfusion microincubator (Medical Systems, Greenvale, NY) on an inverted Leitz microscope equipped with phase-contrast optics. Whole-cell currents were obtained using an Axopatch 200A integrating patch-clamp amplifier (Axon Instruments, Foster City, CA). Cell membrane voltage was stepped from −100 mV to +100 mV in 20 mV increments from a holding potential of −80 mV. Voltage pulses were 820 msec in duration and were delivered once every second. The output of the current-to-voltage converter was lowpass filtered at 300 Hz and then digitally sampled at 625 Hz by a Digidata 1200 A/D converter (Axon Instruments) interfaced with an IBM-compatible computer (AST Premmia 4/66d). Voltage-clamp proto-

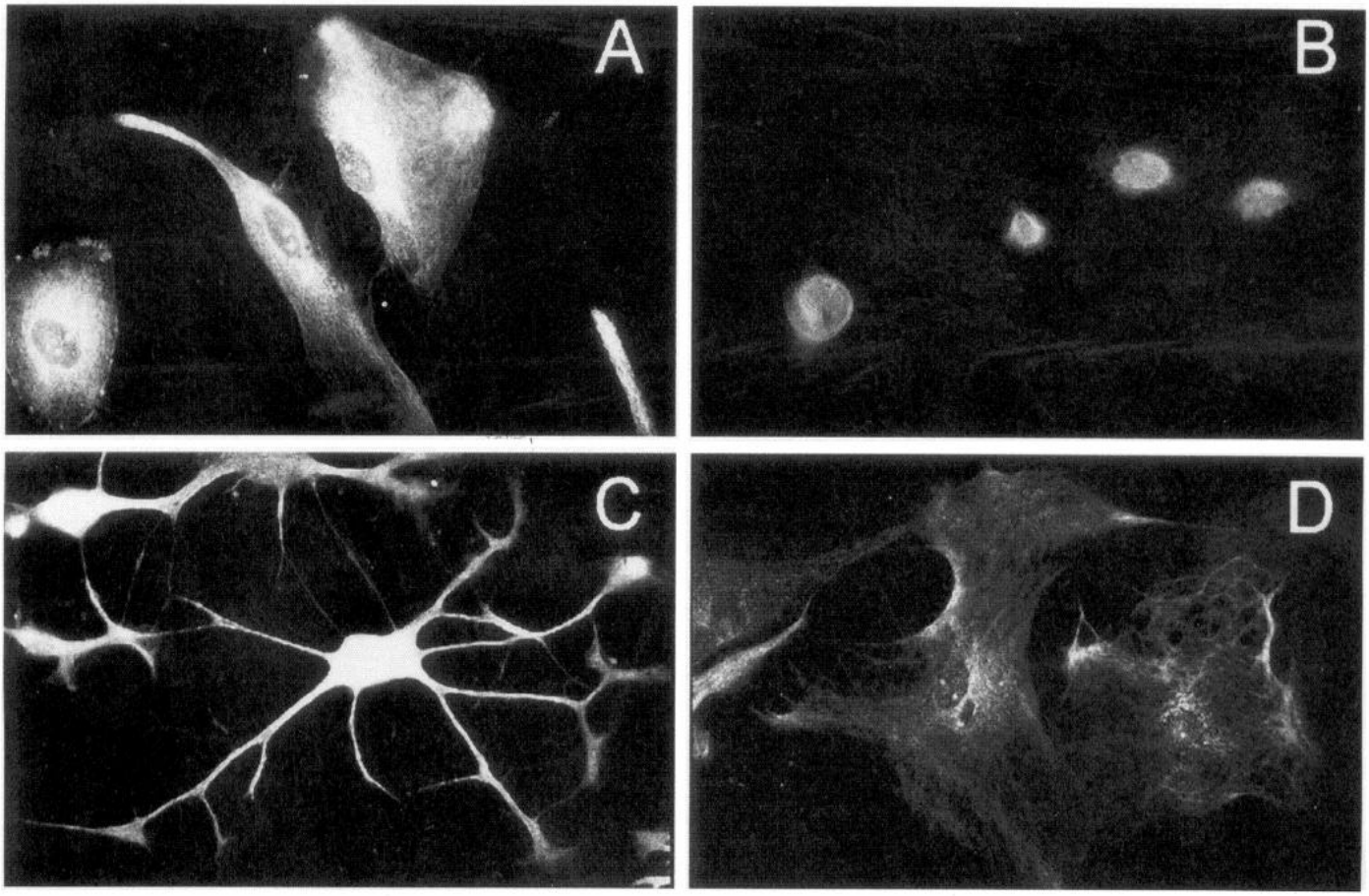

Figure 1. Four astrocytic morphologies in cerebral cortical cultures. *A*, Astrocytes are from a control culture, grown in serum-containing DMEM. Cells were fixed and labeled with a rabbit antiserum to GFAP followed by a rhodamine-conjugated anti-rabbit Ig antibody. The cells have a flat, polygonal morphology. *B*, Astrocytes were exposed to 0.025% trypsin in a divalent cation-free HBSS for 2–5 min and then stained for GFAP. The cells appear as rounded-up spheres 10–20 μM in diameter. *C*, Astrocytes were incubated in a standard Ringer's solution (140 NaCl, 10 mM dextrose) for >1 hr at 37°C and labeled with anti-GFAP as above. The morphological transformation included cytoplasmic retraction, rounding-up of the cell body, and the formation of multipolar processes. These changes were most dramatic in cells 3–12 d after secondary plating and when fresh media was given 24 hr before incubation. *D*, Astrocytes were osmotically swollen by exposure to hypotonic media (185 vs 290 mOsm) and stained for GFAP. Total magnification is 387× for each image.

col, data acquisition, storage, and analysis were performed using the pClamp software suite (Axon Instruments).

Cells were equilibrated in bath recording solution before recording. After membrane rupture, large, voltage-dependent K^+ currents (Bevan et al., 1985) were either absent or rapidly decayed to zero in <30 sec as NMDG was exchanged for residual monovalent cations. All ions and pharmacological reagents used were of a MW <1000; complete exchange of reagents was assumed to take place within 2–3 min (Pusch and Neher, 1988). The start of experiments after membrane rupture was therefore delayed 3 min. To avoid subtracting out ohmic regions of chloride current, currents were neither leak- nor capacity-corrected. Capacitance (CAP) and series resistance (SR), however, were monitored frequently throughout experiments to ensure adequate exchange of ions and pharmacological agents as well as to avoid the confounding influence that changing CAP and SR may have on current amplitudes and reversal potentials. CAP and SR estimates were obtained using the compensation circuits on the Axopatch 200A. In cells with little whole-cell current, CAP was also measured by integrating the current during a 20 mV voltage step and subtracting a baseline established ~15 msec after the step (n = 10). These measurements indicated that there was <5% error between the values obtained off the amplifier and those calculated from the charging transients. To minimize junction potential errors, 1 M KCl agar bridges were used as grounds and were refreshed frequently. Solution changes produced a <3 mV junction potential, and therefore correction of data for junction potential offsets was not performed.

Statistics. Data were expressed as mean ± SEM, unless otherwise noted. Student's t test for one population was used to evaluate significance for single groups with respect to zero. Student's independent t test for two populations was used to evaluate significance between groups.

Materials. All salts and pharmacological reagents were purchased from Sigma (St. Louis, MO). Fetal calf serum for culture media was obtained from Gibco (Grand Island, NY).

RESULTS

Astrocyte morphology

Four astrocytic morphologies were studied for expression of Cl^- currents. The first pattern, the control morphology, was seen in cells as they were cultured in the presence of serum-containing DMEM. These cells were flat, thinly spread out, and polygonally shaped when plated either in plastic tissue culture flasks or on glass coverslips. The cells stained positively for GFAP and negatively for A2B5 and are illustrated in Figure 1*A*. The second pattern consisted of cells "rounded up" by briefly (3–5 min) exposing cells to divalent cation-free HBSS containing 0.025% trypsin. The cells, still attached to coverslips, appeared as crinkled spheres 10–20 mM in diameter (Fig. 1*B*). The third pattern, a multipolar process-bearing morphology ("stellate"), was obtained by incubating astrocytes in serum-free Ringer's solution warmed to 37°C for at least 1 hr (Fig. 1*C*). This shape, similar to astrocyte morphology *in vivo*, also has been described for astrocytes cocultured with neurons (Hatten, 1985) or treated with cAMP analogs such as dibutyryl cAMP (dBcAMP) (Lim et al., 1976), phorbol esters (Mobley et al., 1986), or the kinase inhibitors staurosporine

(Mobley et al., 1994) and H7 (Bedoy and Mobley, 1989). After exposure to warm Ringer's solution, these cells underwent retraction of cytoplasm and process elongation as early as 20 min after exposure, with most cells transformed within 1–3 hr. The rate of morphological transformation was fastest when DMEM was refreshed 24 hr before incubation in Ringer's solution that was made fresh the same day, and it did not depend on whether a HEPES or a HCO_3/CO_2 system was used to buffer pH. The fourth shape change comprised cells osmotically swelled by exposure to hypotonic solution (Fig. 1*D*). The recording solution, normally set at 290 mOsm, was made hypo-osmotic (185 mOsm) by diluting the NMDG-Cl component.

Cl^- currents are not present in flat astrocytes

To determine whether rat neocortical astrocytes in culture expressed whole-cell Cl^- currents, pipette and bath recording solutions were designed to eliminate the contribution of monovalent cation currents. Thus all bath and pipette K^+ and Na^+ was replaced with the large impermeant cation $NMDG^+$. We also used bath and pipette solutions with asymmetrical [Cl^-] (140 mM, bath; 40 mM, pipette) to distinguish leakage currents from Cl^- conductance. The Cl^- current reversal potential approximated by the Nernst relationship was −31 mV. In these solutions, whole-cell patching for up to 45 min of flat, polygonal astrocytes in culture revealed no significant conductance of any kind (n = 26) (Fig. 2). Our criteria for a null conductance was a maximum current amplitude of <100 pA at a membrane potential of 100 mV. Cell input resistance in flat, polygonal astrocytes was usually >1.5 GΩ.

Cl^- currents are present in rounded-up cells

The absence of detectable Cl^- currents corroborated several reports examining whole-cell conductances in cultured astrocytes (Nowak et al., 1987; Barres et al., 1990a; Corvalan et al., 1990), but did not support the observation by Bevan et al. (1985) and Gray and Ritchie (1986) of a whole-cell, 4,4-diisothiocyanostilbene-2,2′-disulfonic acid (DIDS)-sensitive Cl^- current in neocortical astrocytes. They described their current as voltage-gated, activated at potentials more positive than −40 to −50 mV, and virtually abolished on replacement of Cl^- with the large anion gluconate. In their experiments, astrocytes were rounded up by exposing the cells to a trypsin-containing divalent cation-free solution with EDTA for 2–5 min to facilitate whole-cell patching. We reproduced more closely these conditions by exposing normally flat astrocytes to divalent cation-free HBSS containing 0.025% trypsin before introducing cells to the recording bath. In these balled-up astrocytes, we observed in 17 of 18 cells outwardly rectifying whole-cell Cl^- currents with an average peak amplitude of 420 ± 73 pA (range = 110-1112 pA; n = 17) at +100 mV and an average current reversal potential of −28.0 ± 0.8 mV (n = 17) (Fig. 3). The current reversal of this conductance shifted 90% of the predicted Nernst for Cl^- when bath [Cl^-] was changed to 40 mM (0.2 ± 2.7 mV; n = 4) and 75% when the [Cl^-] was 8 mM (24.8 ± 2.3; n = 5) by replacement of Cl^- with gluconate (Fig. 3*B*). The current was inhibited significantly by 1 mM Zn^{2+} (n = 3) and 200 μM DIDS (n = 3) (Fig. 7), both known anion channel blockers (Hille, 1992).

One notable difference between our results and those of Gray and Ritchie (1986) was the apparent voltage independence of our chloride currents. Although we observed an outward rectification when the bath and pipette contained 140 mM [Cl^-] and 40 mM [Cl^-], respectively, the whole-cell current–voltage (*I-V*) became linear when the bath and pipette [Cl^-] both equaled 40 mM (Fig. 3*B*). When the bath [Cl^-] was reduced further to 8 mM, the whole-cell current usually became inwardly rectifying (Fig. 3*B*). This behavior of outward and then inward rectification is what may be expected for the asymmetrical distribution of a permeable species as predicted by the constant field equation (Goldman, 1943). Although we did record some heterogeneity in the degree of relative outward to inward rectification (Fig. 6), we always observed a linear *I–V* relationship when bath and pipette solutions were symmetrical at 40 mM [Cl^-]. This suggests a predominantly ohmic rather than a voltage-gated conductance.

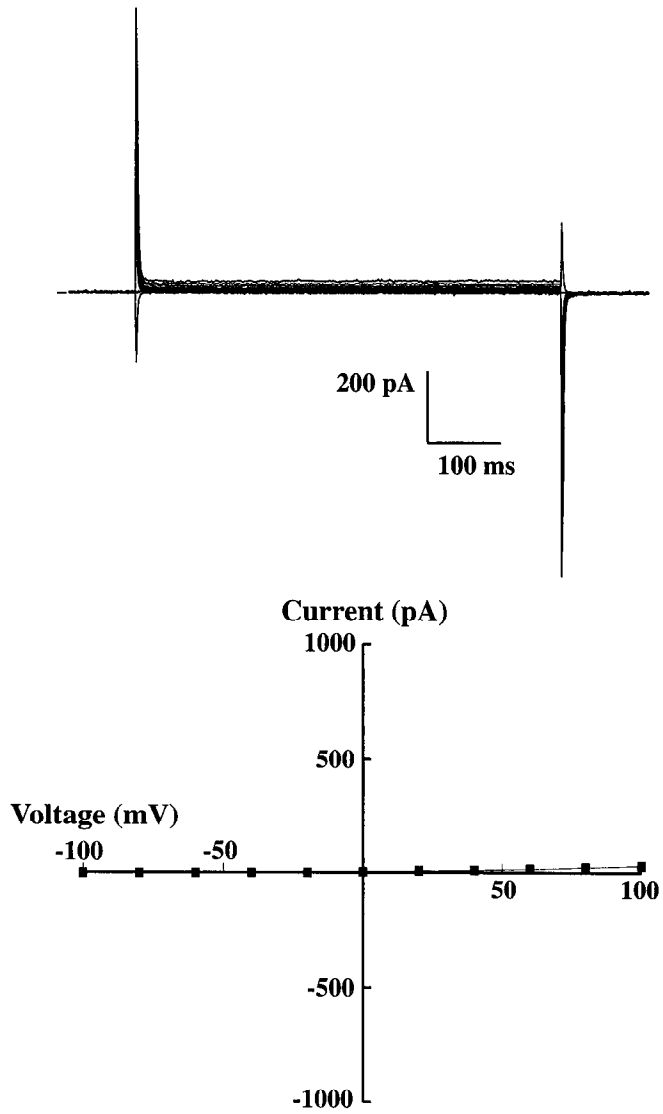

Figure 2. Cells from control cultures do not express whole-cell Cl^- currents. Cl^- currents were not expressed in flat, polygonal astrocytes introduced directly into recording solutions from serum-containing DMEM (n = 26). The bath and pipette recording solutions were designed to eliminate cation currents by replacing all monovalent cations with NMDG. Cell membrane potential was stepped from −100 mV to 100 mV in 20 mV increments. Astrocytes expressing "no conductance" were defined as those cells exhibiting a peak current amplitude of <100 pA at 100 mV. In flat, control astrocytes, input resistance with NMDG-Cl bath and pipette solutions was typically >1.5 GΩ.

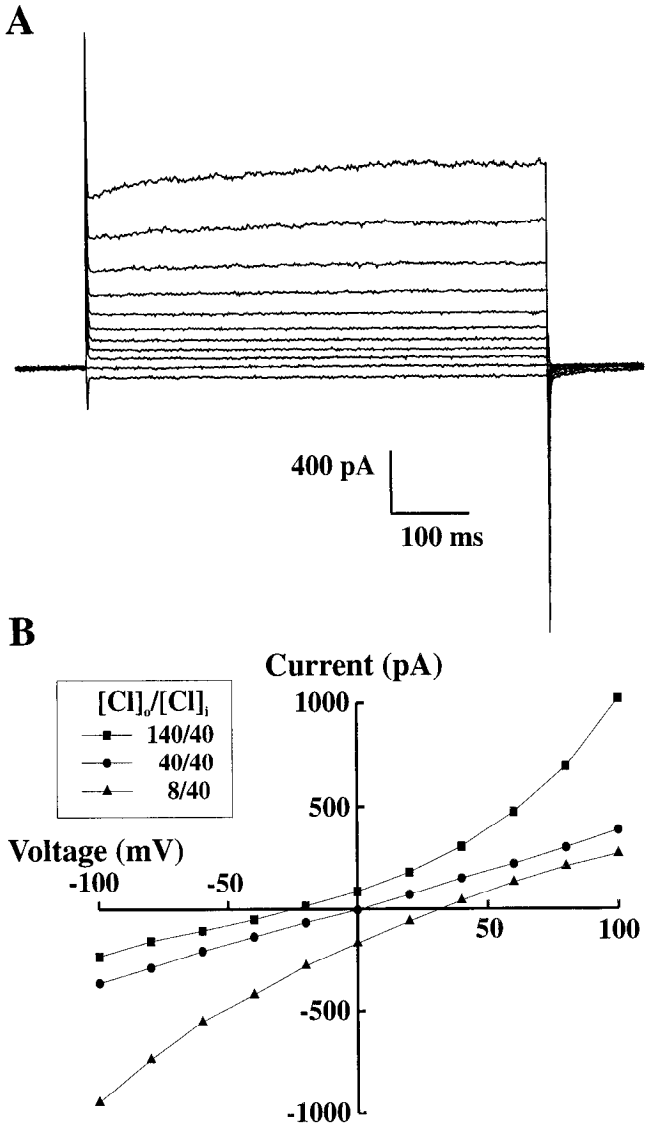

Figure 3. Induction of whole-cell Cl^- currents after cell rounding. *A*, After exposure to 0.025% trypsin in divalent cation-free HBSS, 17 of 18 cells expressed outwardly rectifying whole-cell Cl^- currents in asymmetrical solutions ($[Cl^-]$ = 40 mM in the pipette; 140 mM in the bath). The average peak amplitude at 100 mV was 420 ± 73 pA (n = 17). *B*, The *I–V* relationships of whole-cell Cl^- currents when pipette $[Cl^-]$ was 40 mM and bath $[Cl^-]$ was 140 mM, 40 mM, and 8 mM. Bath Cl^- was replaced with equimolar amounts of gluconate. The average zero-current potential at 140 mM (■) was −28.0 ± 0.8 mV (n = 17), at 40 mM (●) was 0.2 ± 2.7 mV (n = 4), and at 8 mM (▲) was 24.8 ± 2.3 mV (n = 5). At each concentration, *I–V* profiles were outwardly rectifying, linear, and inwardly rectifying, respectively.

Ca^{2+} rarely activates Cl^- current in control astrocytes

We next investigated potential mechanisms for Cl^- current activation after cell rounding-up. We first tested whether the Cl^- conductance was Ca^{2+}-activated, because we suspected that astroglial $[Ca^{2+}]_i$ increased significantly after first exposure to Ca^{2+}-free solution (with trypsin) and then reexposure to media with 2.0 mM $[Ca^{2+}]$ (our recording solution). Ca^{2+} removal followed by Ca^{2+} replacement produces a "calcium paradox" in astrocytes and other cells (Uemura et al., 1985; Kim-Lee et al., 1992) in which $[Ca^{2+}]_i$ levels increase dramatically above their original resting baseline. Ca^{2+} has been shown to activate Cl^- channels via calmodulin kinase II (Holevinsky et al., 1994) as well as directly in oocytes (Miledi and Parker, 1984). In addition, activation of protein kinase C, most isoforms of which are Ca^{2+}-dependent, has also been demonstrated to induce Cl^- currents (Schumann and Raffin, 1994). In recordings lasting up to 30 min, we observed detectable Cl^- currents when patching with a pipette $[Ca^{2+}]$-buffered to 2000 nM in only 2 of 15 flat astrocytes (13%, as compared with 94% of rounded-up cells; data not shown). This result suggested that although Ca^{2+} may have a role in activating Cl^- currents, elevated Ca^{2+} alone was usually insufficient, and other additional intracellular factors might be involved in current expression.

Stellate astrocytes express Cl^- current

We also tested for activation by protein kinase C by exposing cells to 1 μM phorbol 12-myristate 13-acetate (PMA) in serum-free Ringer's solution at 37°C for 1 hr. After this incubation, we observed in four of five cells outwardly rectifying Cl^- currents (595 ± 283 pA, data not shown). Yet when we pretreated cells with PMA and staurosporine, a general kinase inhibitor, we also observed Cl^- current in four of four cells (471 ± 189 pA, data not shown). Finally, when we ran the control, incubating the cells in Ringer's solution alone with no PMA or staurosporine at 37°C for 1 hr, the next five cells also exhibited outwardly rectifying whole-cell Cl^- currents (data included in a larger set below) (Fig. 4).

In the PMA and PMA plus staurosporine-treated populations, and in the control population incubated in Ringer's solution alone, the astrocytes had undergone dramatic morphological changes. Cells changed from a flat, polygonal morphology to one in which the cell body was rounded up with multiple processes (Fig. 1*C*). In cells transformed by exposure to only warm Ringer's solution, cell capacitance (as an approximation of cell size) ranged from 23 to >100 pF with a mean of 61 ± 21 pF (n = 46). Thus these transformed cells varied in size and on the whole were large. In 46 cells exposed to warm Ringer's solution alone, 89% (41 of 46) of process-bearing astrocytes expressed whole-cell Cl^- currents (Fig. 4), with a mean peak amplitude of 598 ± 77 pA (range = 111-1935 pA) at +100 mV. Amplitude correlated poorly with cell capacitance (r = 0.25, by least squares linear regression). The current reversal potential for these cells was −29.9 ± 0.8 mV (n = 5) with 140 mM $[Cl^-]$ in the bath and 40 mM $[Cl^-]$ in the pipette. With 40 mM $[Cl^-]$ in both the bath and pipette, the reversal potential was 8.6 ± 2.2 mV (n = 5), and the *I–V* was again linear (Fig. 4*B*). With 8 mM $[Cl^-]$ in the bath, the reversal depolarized to 31 ± 2.6 mV (n = 4), and the *I–V* became inwardly rectifying (Fig. 4*B*). These currents were also significantly inhibited by 1 mM Zn^{2+} (n = 3) as well as 200 μM DIDS (n = 3) (Fig. 7).

Swelling activates Cl^- current

Although a role for second messenger systems in Cl^- current activation in both rounded-up and stellate astrocytes could not be ruled out, no obvious Ca^{2+}-dependent messenger system or kinase pathway seemed to be required through activation by direct increases in $[Ca^{2+}]_i$ or application of pharmacological agents. The property that both the "balled up" and the process-bearing astrocytes shared was significant change in cell shape. We therefore investigated whether another cell structural perturbation, osmotic swelling, could also elicit Cl^- current. After exposure to a recording solution with a reduced osmolarity of 185 mOsm (normally 290 mOsm), 8 of 10 cells expressed whole-cell Cl^- currents with a mean peak amplitude similar to that in rounded-up and trans-

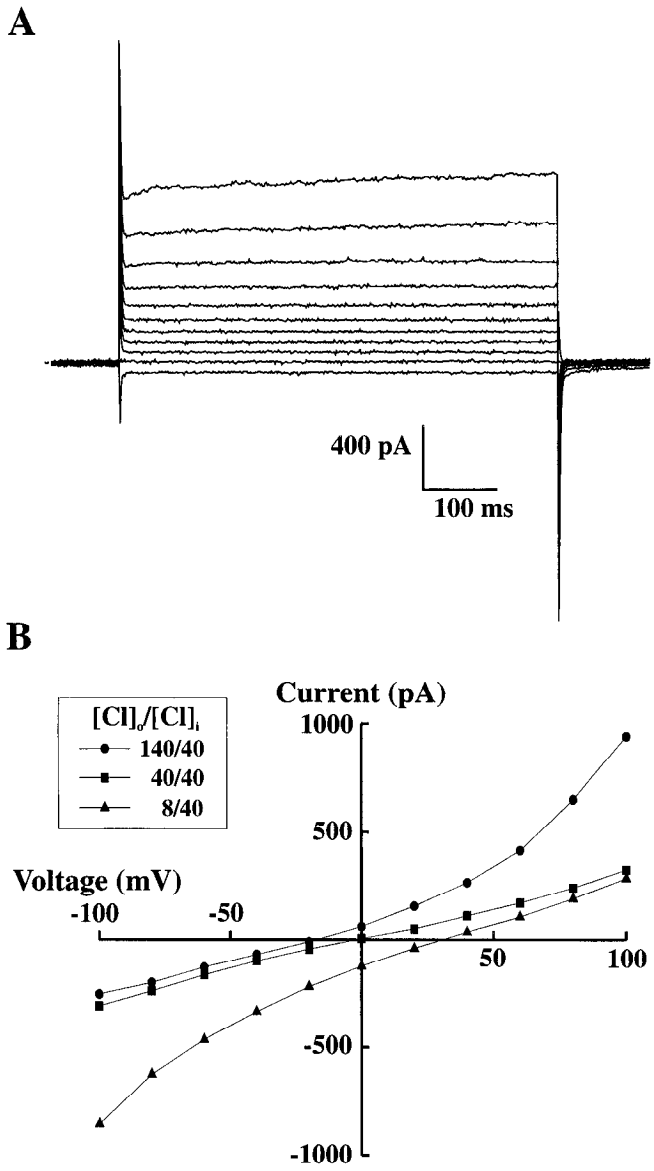

Figure 4. Stellate astrocytes express Cl^- currents. *A*, After incubating flat astrocytes in Ringer's solution for >1 hr at 37°C, cells were transformed into a process-bearing morphology, and 89% (41 of 46 cells) expressed whole-cell Cl^- currents with an average peak amplitude at 100 mV of 598 ± 77 pA (n = 41). Expression did not depend on activation by protein kinase C using phorbol esters (PMA), on the presence of the kinase inhibitor staurosporine, or on whether a bicarbonate or a HEPES-based buffer system was used. *B*, *I–V* profiles at different bath [Cl^-], generated as in Figure 3. The zero-current potential at 140 mM (●) was −29.9 ± 0.8 mV (n = 41), at 40 mM (■) was 8.6 ± 2.2 (n = 5), and at 8 mM (▲) was 31 ± 2.6 mV (n = 4). As with the rounded-up cells, the *I–V* is rectifying in asymmetrical solutions and linear when bath and pipette [Cl^-] are both 40 mM.

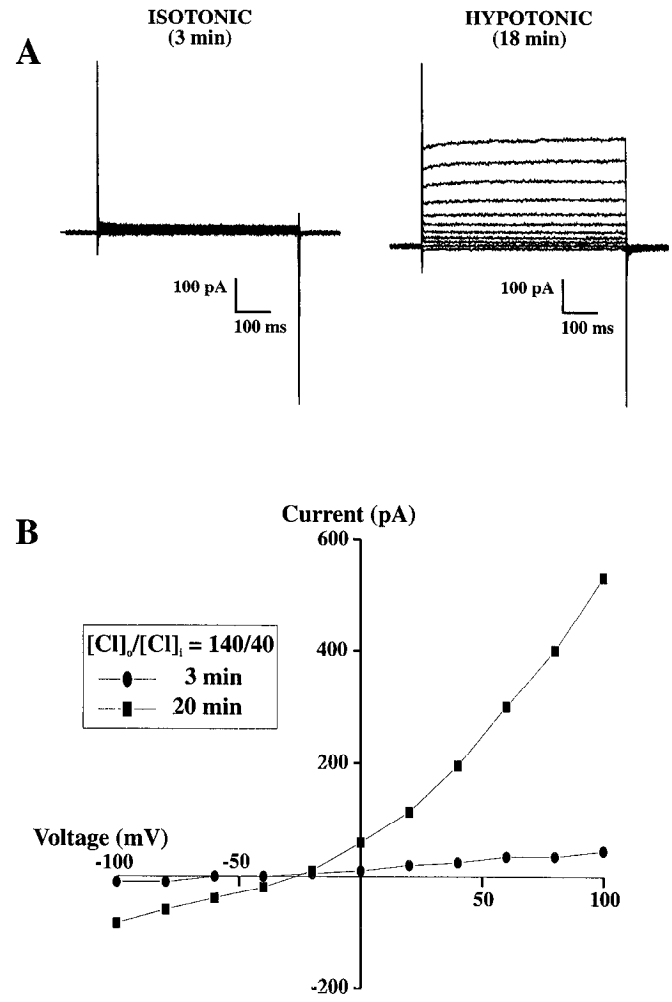

Figure 5. Cell swelling activates a Cl^- conductance. *A*, Whole-cell Cl^- currents were present in 8 of 10 cells exposed to hypotonic (185 mOsm; normally 290 mOsm) recording solutions. Bath osmolarity was reduced by selectively diluting the NMDG-Cl component of the bath solution while maintaining [Ca^{2+}], [Mg^{2+}], and [HEPES]. The average peak amplitude in 8 cells was 410 ± 101 pA after the bath solution was changed back to 290 mOsm (140 mM NMDG-Cl). *B*, The whole-cell currents at 140 mM bath [Cl^-] (■) were outwardly rectifying, and the average zero-current potential was −30.0 ± 1.8 mV (n = 8). *Filled ovals* indicate cells 3 min after whole-cell configuration was achieved and before osmotic change.

formed cells (410 ± 101 pA; n = 8) (Fig. 5). Bath osmolarity was reduced by selectively diluting the NMDG-Cl component of the bath, and [Ca^{2+}], [Mg^{2+}], and [HEPES] were kept constant. The current reversal followed the Nernst prediction when the concentrations of bath NMDG and Cl^- were returned to 140 mM (−30.0 ± 1.8 mV; n = 8) (Fig. 5*B*). When the bath [NMDG] and [Cl^-] was reduced but supplemented with sucrose to maintain osmolarity, no current was evident (n = 5, data not shown). The swelling-activated current also shared the same Zn^{2+} (n = 3) and DIDS (n = 3) pharmacology as the Cl^- currents expressed in the balled-up and process-bearing astrocytes described above (Fig. 7).

Heterogeneity of chloride currents

In all three morphological paradigms, i.e., rounded up, process bearing, and osmotically swelled, we observed variability in both voltage- and time-dependent activation and inactivation. As illustrated from the current traces of three cells in Figure 6*A*, current kinetics could vary from a delayed activation (*left-hand current trace* in Fig. 6*A*) to an instantaneous, time-independent activation (*middle record* in Fig. 6A). Although activation in most cells of all three morphologies tended toward time-independent activation, different cells expressed activation kinetics along the entire spectrum, from instantaneous to delayed. In addition, activation ki-

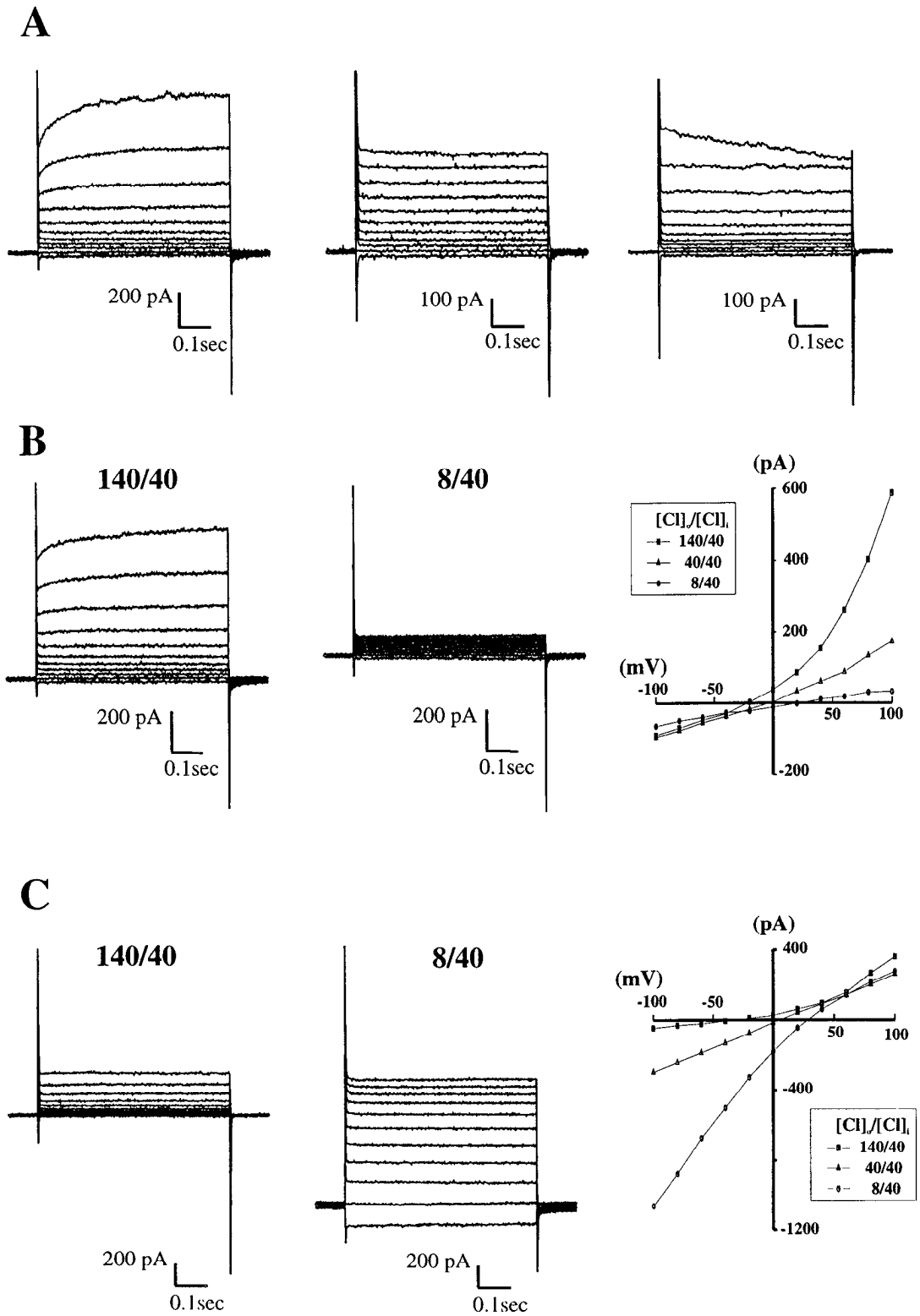

Figure 6. Heterogeneity of astroglial Cl^- currents. *A*, Variability in the kinetics of current activation and inactivation were seen in each morphological paradigm. The *left-hand profile* shows whole-cell currents with a delayed activation, most apparent at depolarized potentials. The *middle* and *right traces* demonstrate currents with instantaneous activation. The *right trace*, as compared with the *middle* and *left-hand traces*, shows depolarization-dependent inactivation, most evident at 100 mV. Variability in activation and inactivation kinetics could be seen within single cells and across cells in each morphology. Each variation was seen in every cell shape in which Cl^- currents were expressed. *B* and *C*, Variability was also observed in the degree of outward relative to inward rectification when zero-current potentials were examined by replacing bath Cl^- with gluconate. These observations were made in rounded-up and stellate cells. Although the absolute magnitudes of outward relative to inward rectification were usually approximately equal, the cell in *B* demonstrates an extreme example of dominant outward rectification, and the cell in *C* demonstrates the most extreme example of dominant inward rectification.

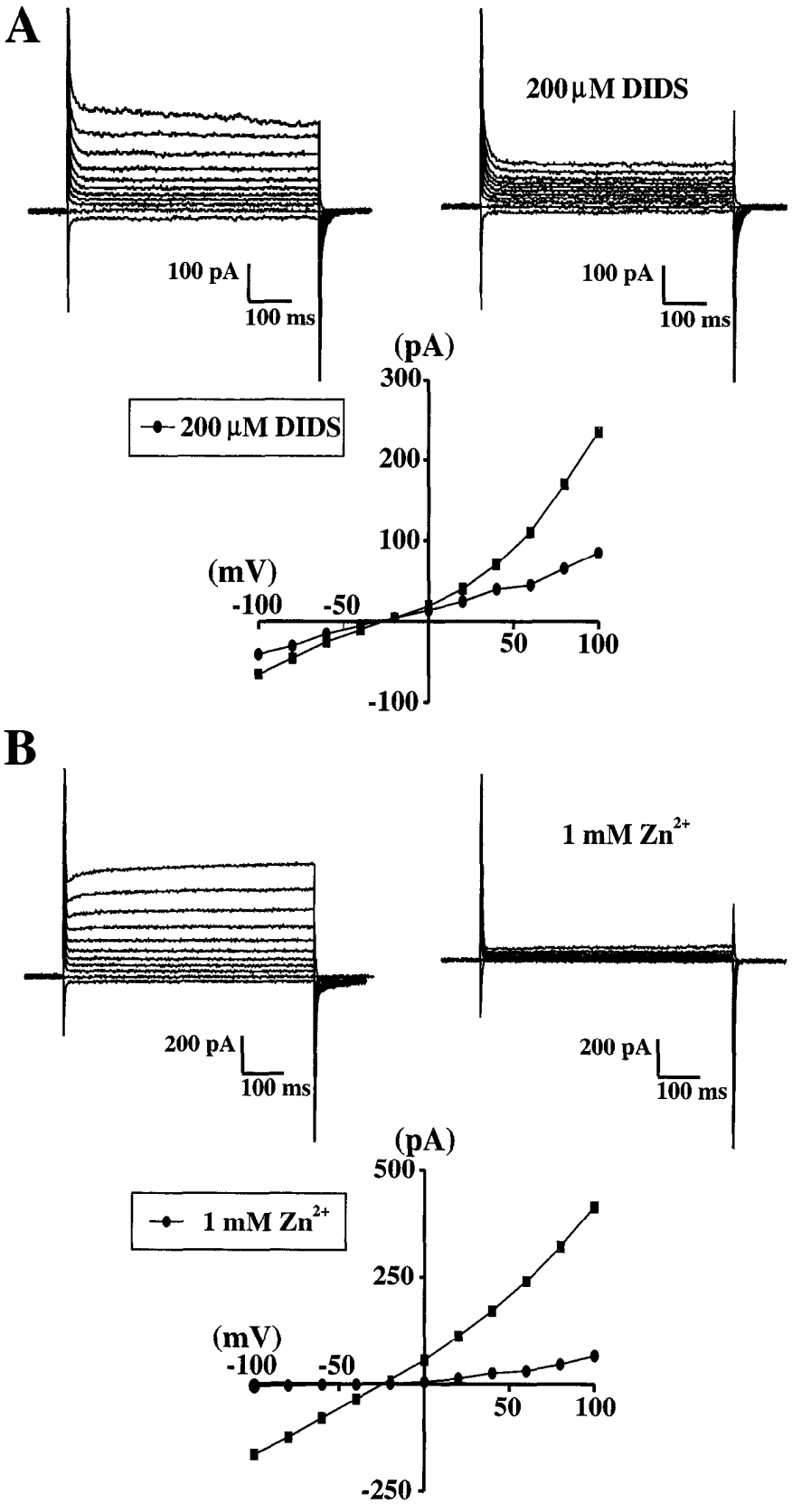

Figure 7. Cl^- currents are inhibited by Zn^{2+} and DIDS. *A*, Whole-cell Cl^- currents expressed in each experimental condition were inhibited (74 ± 12%; $n = 12$) by 200 μM DIDS. Peak *I–V* relationship in a stellate cell before (■) and after (●) application of DIDS. *B*, Cl^- currents were also blocked (87 ± 5%; $n = 12$) by 1 mM Zn^{2+}. Peak *I–V* profile for a stellate cell before (■) and after (●) Zn^{2+} application. The pharmacology was the same across experimental paradigms. DIDS block was only partially reversible, whereas Zn^{2+} block was completely reversible 5–10 min after washout.

netics could shift within a single cell over time, with the shift in current kinetics almost always from delayed activating to time-independent. We also observed a time-dependent delayed inactivation at depolarized potentials in 10–20% of cells from all three paradigms (Fig. 6*A*, *right-hand current trace*). Again, as with activation, there was considerable variability in the degree of time-dependent inactivation, and the degree of inactivation could shift during recording, most often from no inactivation to considerable inactivation at +80 to +100 mV. Depolarization and time-dependent inactivation in swelling-induced Cl^- currents in rat glioma cells has been studied recently in detail (Jackson and Strange, 1995).

Another type of heterogeneity in current profiles became evident as we sequentially reduced bath [Cl^-] while recording from rounded-up and process-bearing astrocytes. Although the *I–V* profiles were always linear when bath and pipette [Cl^-] were both 40 mM, the degree of outward rectification relative to inward rectification varied from cell to cell when the bath [Cl^-] was either 140 mM or 8 mM. The two extremes are illustrated in Figure 6*B,C*. Thus some cells had a dominant outward rectification when the bath [Cl^-] was 140 mM and virtually no inward rectification at 8 mM [Cl^-] (Fig. 6*B*), even as the zero-current potential accurately followed the predicted $Nernst_{Cl^-}$. In other cells the opposite held (Fig. 6*C*), with the relative magnitude of inward rectifying current at 8 mM bath [Cl^-] greater than the magnitude of outward rectifying current at 140 mM [Cl^-]. This type of heterogeneity, as well as that in activation and inactivation kinetics, suggests (1) an underlying diversity in astrocytic Cl^- channels and/or (2) a homogenous population of channels at different states of modulation, perhaps via different degrees of phosphorylation.

Cytoskeletal actin and Cl^- currents

When astrocytes undergo cytoplasmic retraction, cell-body rounding, and process development and elongation after exposure to cAMP analogs, these shape changes are associated with the rapid depolymerization and breakdown of actin (Goldman and Abramson, 1990; Baorto et al., 1992). Although our cells were not exposed to cAMP analogs, the morphological changes after exposure to serum-free Ringer's solution were similar to those reported after incubation with dBcAMP or agents such as forskolin (Barres et al., 1989), which activate adenylate cyclase. This evidence, combined with that demonstrating a role for actin depolymerization in cell swelling (for review, see Mills et al., 1994) and in the modulation of Ca^{2+} (Johnson and Byerly, 1993), NMDA (Rosenmund and Westbrook, 1993), Na^+ (Cantiello et al., 1991), and Cl^- channel activity (Schwiebert et al., 1994) led us to test the hypothesis that depolymerization of cytoskeletal actin mediates the expression of Cl^- currents accompanying changes in astrocytic morphology.

Inclusion of 5 μM cytochalasin B (n = 6), cytochalasin D (n = 4), or dihydrocytochalasin B (n = 3), which depolymerizes actin by augmenting actin-ATP hydrolysis (Sampath and Pollard, 1991), elicited whole-cell Cl^- currents in flat, polygonal control cells otherwise not expressing any significant conductance (Fig. 8). Average peak current amplitude pooled for all cytochalasins used was 420 ± 108 (n = 13), and the zero-current potential was −28.4 ± 0.9 mV. In most cells, Cl^- current was evident within 3 min after achieving the whole-cell configuration and usually became maximal 10–20 min after the start of the experiment. Differences in the time course of activation may be attributable to cell-to-cell variability in access resistance as well as cell size. Better estimates of the kinetics of depolymerization and conductance activation

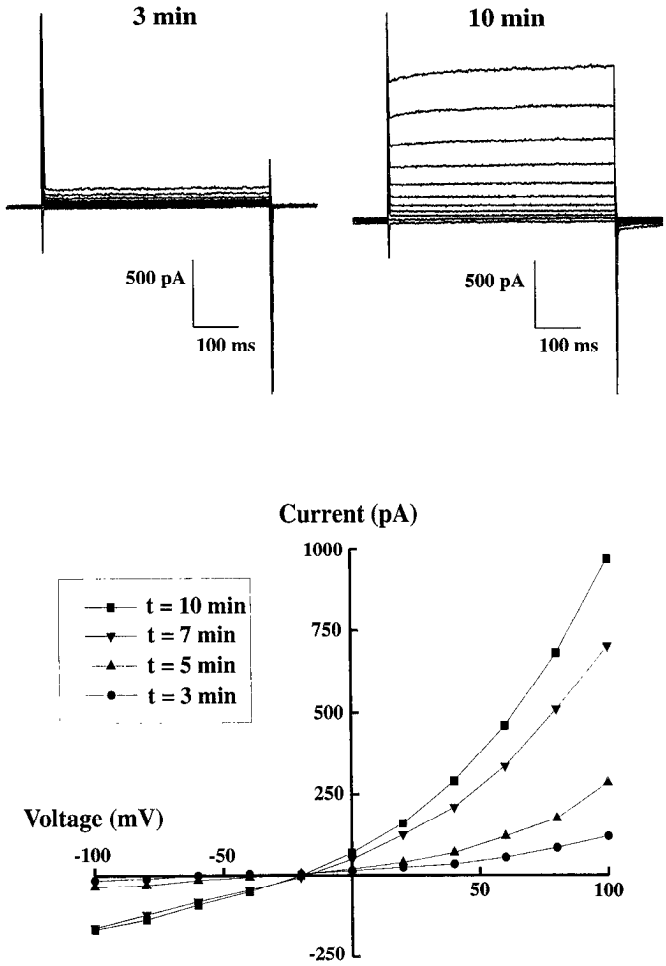

Figure 8. Cytochalasins activate Cl^- currents in control astrocytes. Whole-cell Cl^- currents were elicited in flat, polygonal cells when dialyzed with 5 μM cytochalasin B (n = 6), cytochalasin D (n = 4), and dihydrocytochalasin B (n = 3). Average peak current amplitude for all cytochalasin-treated cells was 420 ± 108 pA (n = 13), comparable to the peak amplitude of Cl^- currents in each morphological transformation. The mean zero-current potential for all cells was −28.4 ± 0.9 mV. Some Cl^- current was usually evident 3 min after going whole-cell and became maximal 10–20 min after the start of the recordings. The cell in this figure expressed peak current at 10 min after the start of the experiment with 5 μM cytochalasin B.

are more likely to be obtained in experiments in which drugs are applied directly to excised patches expressing dormant channels.

In cells, the actin cytoskeleton can be regulated dynamically, with increases in intracellular Ca^{2+} rapidly depolymerizing filamentous actin (F-actin) and ATP (along with other cellular molecules) inducing repolymerization (Pollard and Cooper, 1986). Although in flat, polygonal astrocytes, elevated intracellular Ca^{2+} alone was rarely sufficient to activate Cl^- current, elevated [Ca^{2+}] in stellate cells dramatically enhanced Cl^- currents already present by 187 ± 47% (n = 10) (Fig. 9*A*). The enhancement seemed to be actin-dependent, because co-inclusion in the pipette of 1 μM phalloidin, which binds and stabilizes F-actin, significantly inhibited the Ca^{2+}-induced increase in current (n = 8; $p < 0.005$) (Fig. 9*A*). The percentage current change (−8% ± 5%) from zero with phalloidin was insignificant (p = 0.17) (Fig. 9*A*). Additionally, 5 mM ATP in the pipette produced a decrease in Cl current in stellate cells of 44 ± 10% (n = 8) (see Fig. 9*B*) and was

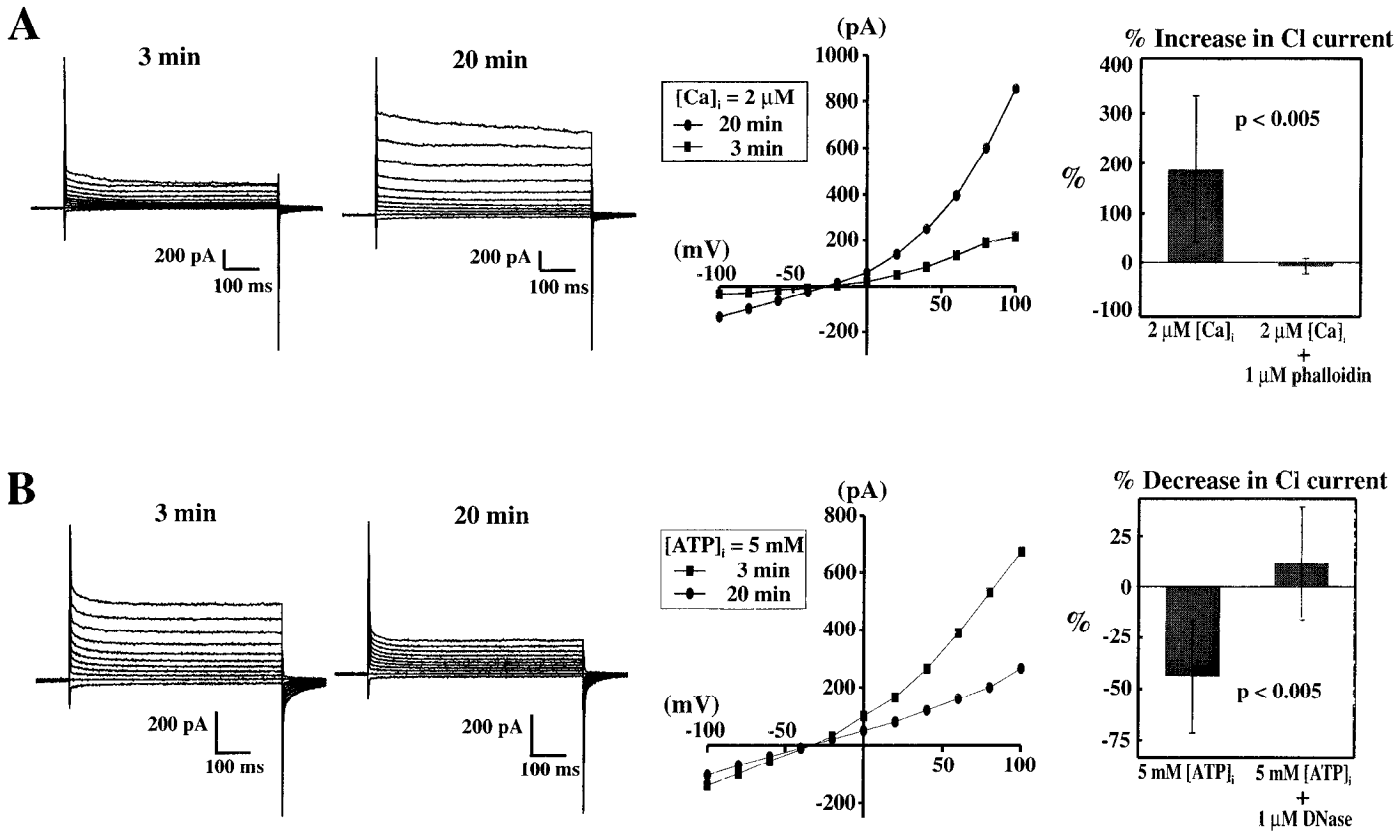

Figure 9. Actin-dependent modulation of Cl^- currents by Ca^{2+} and ATP in stellate cells. *A*, In stellate cells already expressing Cl^- currents, pipette Ca^{2+} buffered to 2 μM amplified Cl^- currents by 187 ± 47% ($p < 0.005$; $n = 10$) during 20 min of recording (●). This amplification was blocked by co-inclusion of 1 μM phalloidin in the pipette ($p < 0.005$; $n = 8$). Percentage current change from zero (−8 ± 5%) with phalloidin in the pipette was insignificant ($p = 0.17$). *B*, In stellate cells, 5 μM pipette ATP significantly reduced Cl^- currents by 44 ± 10% ($p < 0.005$; $n = 8$) (●) over 20 min. This effect of ATP was blocked by co-inclusion with bovine DNaseI ($p < 0.005$; $n = 5$). Percentage current change from zero (11 ± 7%) with DNaseI in the pipette was insignificant ($p = 0.19$).

prevented significantly by codialysis with DNaseI ($n = 5$; $p < 0.005$) (see Fig. 9*B*), which binds tightly to monomeric actin and inhibits polymerization (Kabsch and Vandekerckhove, 1992). The percentage current change from zero (11 ± 7%) with DnaseI was insignificant ($p = 0.19$) (Fig. 9*B*). The effects of Ca^{2+} and ATP, and their prevention by agents that bind actin, suggest strongly that astrocytic Cl^- current can be modulated dynamically by changes in intracellular Ca^{2+} and cell metabolism acting through the actin cytoskeleton.

Finally, we were also able to block osmotically induced Cl^- currents in astrocytes by cell dialysis with 1 μM phalloidin before exposing cells to hypotonic recording solutions ($n = 5$; data not shown). This effect of phalloidin on osmotically activated whole-cell Cl^- currents has been observed recently in renal cells (Schweibert et al., 1994).

Actin cytochemistry

We stained cytoskeletal F-actin in astrocytes using an FITC-conjugate of phalloidin (Faulstich et al., 1988) to provide parallel evidence that the actin cytoskeleton is being altered in cells undergoing morphological changes. In flat untransformed control cells, the F-actin appears in a striking, well organized criss-crossing pattern of stress fibers that traverses the entire cell and intersect with the membrane (Fig. 10*A*). When the cells are rounded up by exposure to trypsin, this organized pattern of actin looks completely disrupted (Fig. 10*B*). The stress fibers are no longer evident, and stained F-actin seems to be collapsed around the nucleus. In cells that have been converted to stellate after exposure to warm Ringer's solution, the stress fiber pattern again looks disrupted, but not as dramatically (Fig. 10*C*). F-actin staining is diffuse throughout the cytoplasm, with remnants of the criss-crossing fibers still visible. Finally, flat control cells osmotically swelled also demonstrate a clear disruption of F-actin (Fig. 10*D*). Actin disruption after osmotic swelling has been show in other cell types as well (Hallows et al., 1991).

DISCUSSION

Our results demonstrate that astrocytic morphology can determine the expression of an electrogenic pathway for Cl^- transport in culture. Furthermore, Cl^- conductances can be open at astrocytic resting potentials, and cytoskeletal actin may have a major role, directly or indirectly, as a mechanism modulating Cl^- channel expression in astrocytes. Finally, astroglial Cl^- currents seem to be modulated by changes in $[Ca^{2+}]_i$ and $[ATP]_i$, which in turn influence the polymerization status of actin. These results are significant because previous studies have shown that Cl^- conductances are normally inactive in cultured astrocytes. Channel activity is observed only after excision of membrane patches. Current-clamp recordings (Kimelberg et al., 1979; MacVicar et al., 1989) and other whole-cell voltage clamp reports (Nowak et al., 1987; Barres et al., 1990a; Corvalan et al., 1990) support these single-channel studies. Several investigators have suggested that the removal of a constitutive inhibitor in astrocytes might be

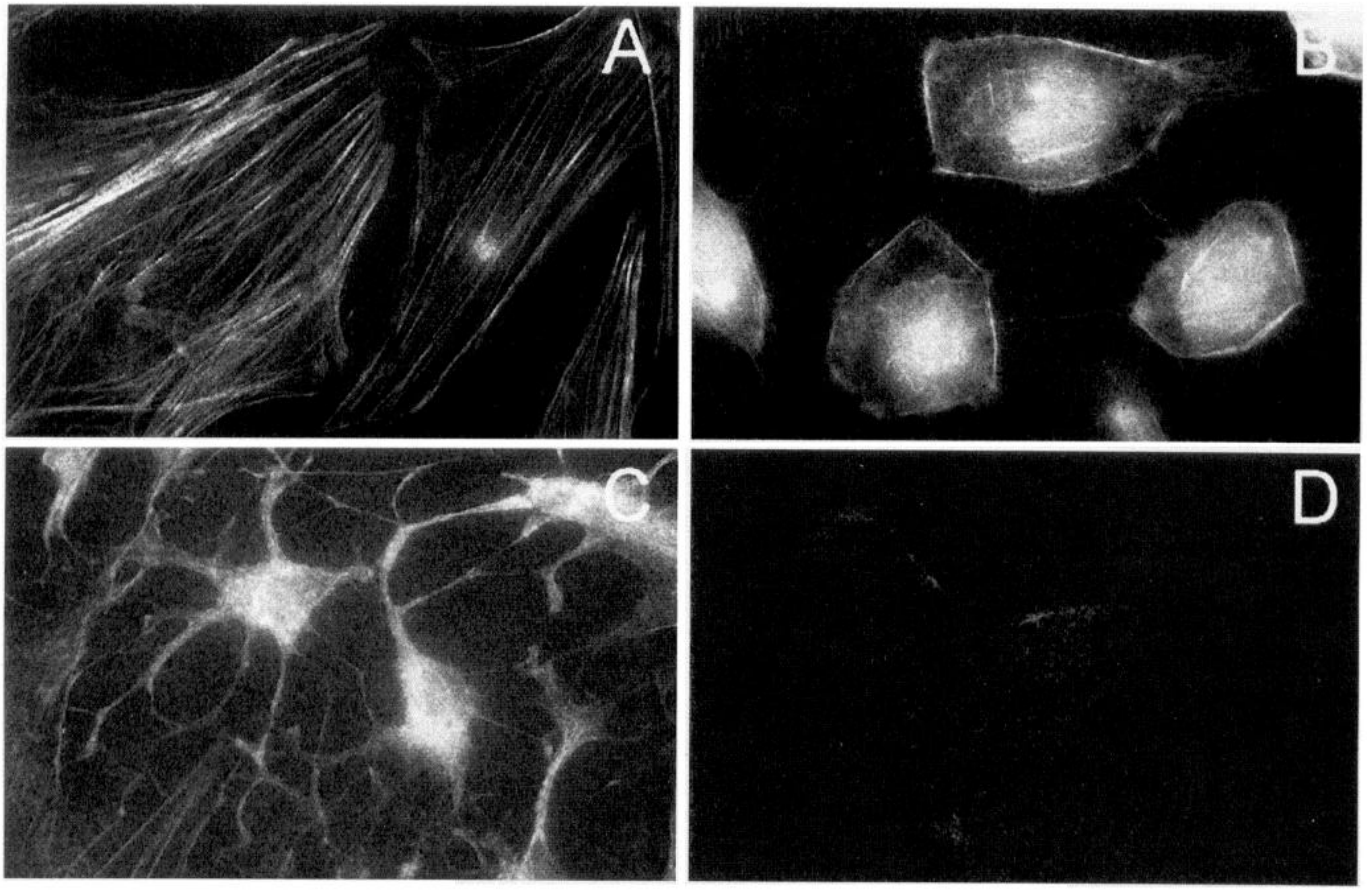

Figure 10. Actin breakdown accompanies morphological change. *A–D*, Cytoskeletal actin from each astrocytic morphology was examined using an FITC conjugate of phalloidin. *A*, Flat, polygonal control astrocytes demonstrate a well organized criss-crossing pattern of stress fibers that traverse the entire cell and meet beneath the membrane surface with cortical actin network parallel to the membrane. *B*, Cells rounded up by exposure to trypsin reveal a complete disruption of organized actin stress fibers. Polymerized actin seems to be present only around the nucleus and underneath the membrane. *C*, Stellate cells transformed from control by exposure to warm Ringer's solution also demonstrate a disruption of the well organized pattern of actin fibers seen in flat, polygonal astrocytes, although cytoplasmic actin polymers seem to be more diffusely present than in rounded-up cells. *D*, Cells exposed to hypotonic (185 mOsm) recording bath for 10 min also demonstrate diffuse depolymerization of actin. Total magnification is 489× for each image.

necessary for Cl^- current expression (Barres et al., 1990b). Our data suggest that polymerized actin may be part of an inhibitory mechanism suppressing channels in quiescent astrocytes. Changes in cell shape, through depolymerization of cytoskeletal actin, may activate normally suppressed Cl^- channels.

Cl^- conductances and cytoskeletal actin

Several reports now exist that demonstrate an interaction between actin depolymerization and ion channel activation. Cytochalasins activate a stretch- and swelling-sensitive large-conductance anion channel in a renal cell line (Schwiebert et al., 1994); RVD and K^+ channel activation depend on the presence of an actin-binding protein in melanoma cells (Cantiello et al., 1993), and disruption of F-actin activates Na^+ channels in A6 cells (Cantiello et al., 1991). Cytochalasins also increase the open probability of an intermediate Cl^- channel in skeletal muscle cells (Haussler et al., 1994) and potentiate the activation of a volume-regulated Cl^- conductance in B-lymphocytes (Levitan et al., 1995). Depolymerization of actin may also be associated with channel rundown and inactivation, however, as has been shown for Cl^- channels (Suzuki et al., 1993), NMDA channels (Rosenmund and Westbrook, 1993), and Ca^{2+} channels (Johnson and Byerly, 1993). The mechanisms by which actin may be influencing channel function are unknown in each case.

In astrocytes, actin breakdown may liberate an inhibitory molecule or allow access of an activating factor or channel-containing vesicles destined to be inserted into the membrane. Polymerized actin could also interact directly with Cl^- channels, inhibiting activity by changing channel conformation or phosphorylating channel proteins via kinases associated with actin polymers; however, actin may also interact with channels indirectly through other cytoskeletal elements. Several studies have shown that ion channels and transporters are structurally linked to actin through spectrin and ankyrin (Drenckhahn et al., 1985; Nelson and Veshnock, 1987; Srinivasan et al., 1988). Whether these linkages affect the function of these proteins is not known. At present, our data do not provide any mechanistic answers linking actin depolymerization to Cl^- channel activation.

Chloride channels underlying chloride conductances

Gray and Ritchie (1986) described their whole-cell Cl^- currents as reflecting a population of voltage-gated Cl^- channels activated at potentials between −50 mV and −40 mV. We propose that the whole-cell Cl^- currents in our rounded-up astrocytes (and also our stellate and swollen cells) are attributable to the same underlying channel population, but we believe this population is more ohmic than voltage-gated. In our experiments, Cl^- current rectification most often approximated the prediction of the constant-

field equation for a channel population at constant permeability (Goldman, 1943) and was notably absent when $[Cl^-]_i$ and $[Cl^-]_o$ were symmetrical. The differences between our results and those of Gray and Ritchie (1986) may be attributable to different voltage protocols; Gray and Ritchie used a leak current subtraction procedure. The effect of leak subtraction on Cl^- conductances has been noted recently for swelling-activated Cl^- currents in oocytes (Ackerman et al., 1994). Leak subtraction can greatly confound *I–V* relationships, zero-current potentials, and steady-state current amplitudes over time if any portion of the *I–V* relationship is linear, which we found to be the case with astroglial Cl^- currents even in asymmetrical solutions. Therefore, our currents were not leak-subtracted.

The heterogeneity we observed in the kinetics of activation and inactivation suggests that multiple types of channels could underlie shape-dependent Cl^- currents in astrocytes. A distribution of kinetic profiles similar to ours has been observed in oocytes (Ackerman et al., 1994), for example, apparently reflecting separate Cl^- channel types. In addition, the heterogeneity of outward relative to inward rectification also suggests that rectifying (as compared with purely ohmic) Cl^- channels may contribute variably to astroglial Cl^- currents. Two rectifying Cl^- channels have been identified in glial cells to date, both of which may contribute to shape-dependent Cl^- currents. The 25–60 pS Cl^- channel observed by Barres et al. (1990a) in cultured optic nerve type-1 astrocytes is outwardly rectifying and has a significant open probability at both negative and positive potentials. The volume-sensitive anion channel described by Jackson and Strange (1995) in C6 glioma cells is also outwardly rectifying and shares the feature of depolarization-dependent inactivation that we observe occasionally in our morphologically changed astrocytes. In addition, Ferroni et al. (1995) recently reported an inwardly rectifying Cl^- conductance in astrocytes conditioned by long-term exposure to dibutyryl cAMP.

The purely ohmic component of astroglial Cl^- currents could potentially arise from the large-conductance anion channels observed in excised patches from both rat and mouse neocortical astrocytes. The function of these channels with an open probability greatest around 0 mV is not known for any cell type in which they have been observed, although Jalonen et al. (1993) suggested that the astrocytic channel serves as an "emergency" Cl^- permeability pathway during massive depolarizations accompanying cell swelling. Two lines of evidence, however, suggest that these channels may function near high astrocytic resting potentials as well. First, Sonnhof (1987) noted that 10–15% of the large-conductance channels he observed were voltage-independent, active at all potentials from −90 mV to 90 mV. Second, asymmetrical Cl^- solutions, with low Cl^- on the intracellular face of the membrane, can shift the open probability curve of large-conductance anion channels by several tens of millivolts in the hyperpolarizing direction (Hals and Palade, 1990). In cultured astrocytes, $[Cl^-]_i$ is 20–40 mM (Kettenmann et al., 1987). In intact tissue, astroglial $[Cl^-]_i$ may be <6 mM (Ballanyi et al., 1987), two orders of magnitude lower than $[Cl^-]_o$. This Cl^- asymmetry could render the entire population of large-conductance channels functional within a more typical range of high astrocyte membrane potentials. In addition, a brain-derived porin sharing many electrophysiological characteristics with large-conductance anion channels has been cloned recently and localized to astrocyte membranes (Dermietzel et al., 1994). Finally, the disruption of F-actin with cytochalasins or by swelling has been shown to activate a large-conductance (305 pS) Cl^- channel in a renal cell line (Schwiebert et al., 1994). The permeability properties, actin-dependence, and function of astrocytic large-conductance anion channels require further investigation.

Significance of shape-dependent Cl^- currents in astrocytes

The induction and modulation of astroglial Cl^- currents through actin depolymerization is likely to influence any process coupled to the movement of anions. One such process is astroglial K^+ homeostasis. During the last 30 years, two competing hypotheses have emerged on how glia regulate extracellular K^+. The first, a "spatial buffering" hypothesis, proposes that elevated K^+ is driven into K^+-selective glial cells and shunted distally by an intraglial voltage gradient (Orkand et al., 1966; Newman, 1984). The second, a "K^+ accumulation" hypothesis, proposes the passive entry of K^+ into glia with anions following as countercharge (Gardner-Medwin, 1980). In the latter scenario, K^+ is stored locally instead, and both uptake and storage necessitate anion permeability.

Several lines of evidence now suggest that K^+ accumulation may be the dominant mechanism by which extracellular K^+ is regulated. Elevations in intracellular K^+ in invertebrate and mammalian glia are accompanied by parallel increases in $[Cl^-]_i$ (Ballanyi et al., 1987; Coles et al., 1989). Cl^--free solutions markedly impede K^+ uptake by glia and disrupt extracellular K^+ regulation in the drone retina (Coles et al., 1989). Intraglial Cl^- measurements using ion-selective microelectrodes in guinea pig olfactory slices suggest that Cl^- is distributed passively (Ballanyi et al., 1987). Finally, Gardner-Medwin (1980) and Barres et al. (1990a) argue that the length constant of adult astrocytes may be too short to support an intraglial voltage gradient sufficient for spatial buffering.

Barres et al. (1990b) have suggested that the K^+ accumulation mechanism dominates everywhere except in the retina, where a spatial buffer process is more anatomically feasible. Our data add support for the K^+ accumulation hypothesis by demonstrating a mechanism for Cl^- permeability; however, our results also suggest that the ability of astrocytes to accumulate K^+ with Cl^- or other anions such as bicarbonate (Kraig and Chesler, 1988) may vary. As seen in our stellate cells, a morphology that more closely resembles that *in vivo*, Cl^- currents seem to be modulated by $[Ca^{2+}]_i$ and $[ATP]_i$ acting through cytoskeletal actin. Perhaps with increased brain activity, elevations in astrocytic $[Ca^{2+}]_i$ trigger an increased Cl^- permeability via actin depolymerization that enhances the capacity of astrocytes to take up K^+ and store it locally. During periods when the brain is relatively quiescent, with $[Ca^{2+}]_i$ low, energy abundant, and actin more polymerized, astroglial Cl^- conductances become markedly decreased, and small local increases in extracellular K^+ are more spatially buffered.

The modulation of astroglial Cl^- currents is also likely to influence other anion-coupled processes, including pH and neurotransmitter homeostasis as well as the control of astrocyte cell volume. Neurotransmitter, pH, and volume aberrations are thought to underlie many disease states in brain. Thus the relationship between structural changes, cytoskeletal alterations, and Cl^- permeability changes is likely to be relevant for how astrocytes behave, not only in physiological but also in pathological contexts. Understanding this relationship could provide important clues about how astrocytes in these contexts interact dynamically with other brain cells and influence not

only their own behavior but also the behavior of their environment.

REFERENCES

Ackerman MJ, Wickman KD, Clapham DE (1994) Hypotonicity activates a native chloride current in *Xenopus* oocytes. J Gen Physiol 103:153–179.

Anderson C (1994) Easy-to-alter digital images raises fear of tampering. Science 263:317–318.

Anderson BJ, Li X, Alcantara AA, Isaacs KR, Black JE, Greenough WT (1994) Glial hypertrophy is associated with synaptogenesis following motor-skill learning, but not with angiogenesis following exercise. Glia 11:73–80.

Backus KH, Berger T, Kettenmann H (1991) Activation of neurokinin receptors modulates K and Cl channel activity in cultured astrocytes from rat cortex. Brain Res 541:103–109.

Ballanyi K, Grafe P, Bruggencate GT (1987) Ion activities and potassium uptake mechanisms of glial cells in guinea-pig olfactory cortex slices. J Physiol (Lond) 382:159–174.

Baorto DM, Mellado W, Shelanski ML (1992) Astrocyte process growth induction by actin breakdown. J Cell Biol 117:357–367.

Barres BA, Chun LLY, Corey DP (1989) Calcium current in cortical astrocytes: induction by cAMP and neurotransmitters and permissive effect of serum factors. J Neurosci 9:3159–3175.

Barres BA, Koroshetz WJ, Chun LLY, Corey DP (1990a) Ion channel expression by white matter glia: the type-1 astrocyte. Neuron 5:527–544.

Barres BA, Chun LLY, Corey DP (1990b) Ion channels in vertebrate glia. Annu Rev Neurosci 13:441–474.

Bedoy CA, Mobley PL (1989) Astrocyte morphology altered by 1-(5-isoquinolinylsulfonyl) 2-methyl piperazine (H-7) and other protein kinase inhibitors. Brain Res 490:243–254.

Bevan S, Chiu SY, Gray PTA, Ritchie JM (1985) The presence of voltage-gated sodium, potassium and chloride channels in rat cultured astrocytes. Proc R Soc Lond [Biol] 225:299–313.

Cantiello HF, Prat AG, Bonventre JV, Cunningham CC, Hartwig J, Ausiello DA (1993) Actin-binding protein contributes to cell volume regulatory i channel activation in melanoma cells. J Biol Chem 268:4596–4

Cantiello HF, Stow J, Prat AG, Ausiello DA (1991) Actin filaments control epithelial Na channel activity. Am J Physiol 261:C882–C888.

Coles JA, Orkand RK, Yamate CL (1989) Chloride enters glial cells and photoreceptors in response to light stimulation in the retina of the honey bee drone. Glia 2:287–297.

Corvalan V, Cole R, deVellis J, Hagiwara S (1990) Neuronal modulation of calcium channel activity in cultured rat astrocytes. Proc Natl Acad Sci USA 87:4345–4348.

Dermietzel R, Hwang TK, Buettner R, Hofer A, Dotzler E, Kremer M, Deutzmann R, Thinnes FP, Fishman GI, Spray DC, Siemen D (1994) Cloning and in situ localization of a brain-derived porin that constitutes a large-conductance anion channel in astrocytic plasma membranes. Proc Natl Acad Sci USA 91:499–503.

Drenckhahn D, Schluter K, Allen DP, Bennett V (1985) Co-localization of band 3 with ankyrin and spectrin at the basal membrane of intercalated cells in the rat kidney. Science 230:1287–1289.

Faulstich H, Zobeley S, Rinnerthaler G, Small JV (1988) Fluorescent phallotoxins as probes for filamentous actin. J Muscle Res Cell Motil 9:370–383.

Ferroni S, Marchini C, Schubert P, Rapisarda C (1995) Two distinct inwardly rectifying conductances are expressed in long term dibutyryl-cyclic-AMP treated rat cultured cortical astrocytes. FEBS Lett 367:319–325.

Froehner S (1991) The submembrane machinery for nicotinic acetylcholine receptor clustering. J Cell Biol 114:1–7.

Gardner-Medwin AR (1980) Membrane transport and solute migration affecting the cell microenvironment. Neurosci Res Program Bull 18:208–226.

Giulian D, Baker TJ (1986) Characterization of ameboid microglia isolated from developing mammalian brain. J Neurosci 6:2163–2178.

Goldman DE (1943) Potential, impedance, and rectification in membranes. J Gen Physiol 27:37–60.

Goldman JE, Abramson B (1990) Cyclic AMP-induced shape changes of astrocytes are accompanied by rapid depolymerization of actin. Brain Res 528:189–196.

Gray PTA, Ritchie JM (1986) A voltage-gated chloride conductance in rat cultured astrocytes. Proc R Soc Lond [Biol] 228:267–288.

Greenfield (1992) Neuropathology, 5th Ed (Adams JH, Duchen LW, eds). New York: Oxford UP.

Guharay F, Sachs F (1984) Stretch-activated single ion channel currents in tissue-cultured embryonic skeletal muscle. J Physiol (Lond) 352:685–701.

Hallows KR, Packman CH, Knauf PA (1991) Acute cell volume changes in anisotonic media affect F-actin content of HL-60 cells. Am J Physiol (Lond) 261:C1154–C1161.

Hals GD, Palade PT (1990) Different sites control voltage dependence and conductance of a sarcoball anion channel. Biophys J 57:1037–1047.

Hamill OP, Marty A, Neher E, Sakmann B, Sigworth F (1981) Improved patch-clamp techniques for high resolution current recordings from cells and cell free membrane patches. Pflügers Arch 391:85–100.

Hatten ME (1985) Neuronal regulation of astroglial morphology and proliferation in vitro. J Cell Biol 104:1353–1360.

Haussler U, Rivet-Bastide M, Fahlke Ch Muller D, Zachar E, Rudel R (1994) Role of cytoskeleton in the regulation of Cl^- channels in human embryonic skeletal muscle cells. Pflügers Arch 428:323–330.

Hille B (1992) Ionic channels of excitable membranes. Sunderland, MA: Sinauer.

Holevinsky KO, Jow F, Nelson DJ (1994) Elevation in intracellular calcium activates both chloride and proton currents in human macrophages. J Membr Biol 140:13–30.

Hudspeth AJ (1989) How the ear's works work. Nature 341:397–401.

Jackson PS, Strange K (1995) Characterization of the voltage-dependent properties of a volume-sensitive anion conductance. J Gen Physiol 105:661–677.

Jalonen T (1993) Single-channel characteristics of the large-conductance anion channel in rat cortical astrocytes in primary culture. Glia 9:227–237.

Johnson BD, Byerly L (1993) A cytoskeletal mechanism for Ca channel metabolic dependence and inactivation by intracellular Ca. Neuron 10:797–804.

Kabsch W, Vandekerckhove J (1992) Structure and function of actin. Annu Rev Biophys Biomol Struct 21:49–76.

Kettenmann H, Backus KH, Schachner M (1987) Gamma-aminobutyric-acid opens Cl channels in cultured astrocytes. Brain Res 404:1–9.

Kimelberg HK, Bowman CL, Biddlecome S, Bourke RS (1979) Cation transport and membrane potential properties of primary astroglial cultures from neonatal rat brains. Brain Res 177:533–550.

Kimelberg HK, Bowman CL, Hirata H (1986) Anion transport in astrocytes. Ann NY Acad Sci 481:334–353.

Kimelberg HK, Rose JW, Barron KD, Waniewski RA, Cragow EJ (1989) Astrocytic swelling in traumatic-hypoxic brain injury. Mol Chem Neuropathol 11:1–31.

Kim-Lee MH, Stokes BT, Yates AJ (1992) Reperfusion paradox: a novel mode of glial cell injury. Glia 5:56–64.

Kraig RP, Chesler M (1988) Dynamics of volatile buffers in brain cells during spreading depression. In: Mechanisms of cerebral hypoxia and stroke (Somjen G, ed), pp 279–289. New York: Plenum.

Kraig RP, Dong L, Thisted R, Jaeger CB (1991) Spreading depression increases immunohistochemical staining of glial fibrillary acidic protein. J Neurosci 11:2187–2198.

Levison SW, McCarthy KD (1991) Astroglia in culture. In: Culturing nerve cells (Banker G, Goslin K, eds), pp 309–336. Cambridge: MIT.

Levitan I, Almonte C, Mollard P, Garber SS (1995) Modulation of a volume-regulated chloride current by F-actin. J Membr Biol 147:282–294.

Lim R, Turriff DE, Troy SS (1976) Response of glioblasts to a morphological transforming factor: cinematographic and chemical correlations. Brain Res 113:165–170.

MacVicar BA, Tse FW, Crichton A, Kettenmann H (1989) GABA-activated Cl channels in astrocytes of hippocampal slices. J Neurosci 9:3577–3583.

Mathewson AJ, Berry M (1985) Observations on the astrocyte response to a cerebral stab wound in adult rats. Brain Res 327:61–69.

McCarthy KD, DeVellis J (1980) Preparation of separate astroglial and oligodendroglial cultures from rat cerebral tissue. J Cell Biol 85:890–902.

Miledi R, Parker I (1984) Chloride current induced by injection of calcium into *xenopus* oocytes. J Physiol (Lond) 357:173–183.

Mills JW, Schwiebert EM, Stanton BA (1994) Evidence for the role of actin filaments in regulating cell swelling. J Exp Zool 268:111–120.

Mobley PL, Hedberg K, Bonin L, Chen B, Griffith OH (1994) Decreased phosphorylation of four 20 kDa proteins precedes staurosporine-induced disruption of the actin/myosin cytoskeleton in rat astrocytes. Exp Cell Res 214:55–66.

Mobley PL, Scott SL, Cruz EG (1986) Protein kinase C in astrocytes: a determinant of cell morphology. Brain Res 398:366–369.
Nakao M, Gadsby DC (1989) [Na] and [K] dependence of the Na/K pump current–voltage relationship in guinea pig ventricular myocytes. J Gen Physiol 94:539–565.
Neher E (1988) The influence of intracellular calcium concentration on degranulation of dialysed mast cells from rat peritoneum. J Physiol (Lond) 395:193–214.
Nelson WJ, Veshnock PJ (1987) Ankyrin binding to (Na + K) ATPase and implications for the organization of membrane domains in polarized cells. Nature 328:533–536.
Newman EA (1984) Regional specialization of retinal glial cell membrane. Nature 309:155–157.
Nowak L, Ascher P, Berwald-Netter Y (1987) Ion channels in mouse astrocytes in culture. J Neurosci 7:101–109.
Orkand RK, Nicholls JG, Kuffler SW (1966) Effect of nerve impulses on the membrane potential of glial cells in the central nervous system of amphibia. J Neurophysiol 29:788–806.
Pasantes-Morales H, Murray RA, Lilja L, Moran J (1994) Regulatory volume decrease in cultured astrocytes I. Potassium- and chloride-activated permeability. Am J Physiol 266:C165–C171.
Petito CK, Morgello S, Felix JC, Lesser MI (1990) The two patterns of reactive astrocytosis in postischemic brain. J Cereb Blood Flow Metab 10:850–859.
Pollard TD, Cooper JA (1986) Actin and actin-binding proteins: a critical evaluation of mechanisms and functions. Annu Rev Biochem 55:987–1035.
Pusch M, Neher E (1988) Rates of diffusional exchange between small cells and a measuring patch pipette. Pflügers Arch 411:204–211.
Ransom B, Kettenmann H (eds) (1995) Neuroglial cells. New York: Oxford UP.
Rosenmund C, Westbrook GL (1993) Calcium-induced actin depolymerization reduces NMDA channel activity. Neuron 10:805–814.
Sampath S, Pollard TD (1991) Effects of cytochalasin, phalloidin, and pH on the elongation of actin filaments. Biochemistry 30:1973–1980.
Schumann MA, Rafflin TA (1994) Activation of a voltage-dependent chloride current in human neutrophils by phorbol 12-myristate 13-acetate and formyl-methionyl-leucyl-phenylalanine. The role of protein kinase C. J Biol Chem 269:2389–2398.
Schwiebert EM, Mills JW, Stanton BA (1994) Actin-based cytoskeleton regulates a Cl channel and cell volume in a renal cortical collecting duct cell line. J Biol Chem 269:7081–7089.
Sonnhof U (1987) Single voltage-dependent K and Cl channels in cultured rat astrocytes. Can J Physiol Pharmacol 65:1043–1050.
Srinivasan Y, Elmer L, Davis J, Bennett V, Angelides K (1988) Ankyrin and spectrin associate with voltage-dependent sodium channels in brain. Nature 333:177–180.
Suzuki M, Miyazaki K, Ikeda M, Kawaguchi Y, Sakai O (1993) F-actin network may regulate a Cl channel in renal proximal tubule cells. J Membr Biol 134:31–39.
Uemura S, Young H, Matsuoka S, Nakanishi T, Jarmakani JM (1985) Calcium paradox in the neonatal heart. Can J Cardiol 1:114–120.
Walz W, Mukerji S (1988) KCl movements during potassium-induced cytotoxic swelling of cultured astrocytes. Exp Neurol 99:17–29.